Electronic Supplementary Material (ESI) for Journal of Materials Chemistry C.

# Electronic Supplementary Information (ESI)

# Magneto-Structural correlations of novel kag MOFs

M. Infas H. Mohideen,*[a] Chen Lei,[a] Jiří Tuček,[b] Ondřej Malina[b], Federico Brivio[a], Valeryia Kasneryk[a], Zhehao Huang[c], Michal Mazur[a], Xiaodong Zou[c], Petr Nachtigall[a], Jiří Čejka[a], Russell E. Morris.[a,d]

[a] *Department of Physical and Macromolecular Chemistry, Faculty of Science, Charles University in Prague, Hlavova 2030, Prague 2, 128 00, Czech Republic.*

[b] *Regional Centre of Advanced Technologies and Materials, Department of Experimental Physics, Faculty of Science, Palacký University in Olomouc, Šlechtitelů 27, 783 71 Olomouc, Czech Republic.*

[c] *Bezerlii Center EXSELENT on Porous Materials, Department of Materials and Environmental Chemistry, Stockholm University, SE-106 91 Stockholm, Sweden.*

[d] *EaStCHEM School of Chemistry, University of St. Andrews, St. Andrews KY16 9ST, Scotland.*

## Table of Contents

1. Materials and general procedures ........ 2
   1.1 Instrumentation ........ 2
   1.2 Experimental Methods ........ 3
2. First principle calculations ........ 4
3. Structural determination and stability ........ 6
4. Thermogravimetric analysis ........ 10
5. AC Magnetic Susceptibility Measurements ........ 11
6. Electronic Structure ........ 13
7. Low Pressure Gas Adsorption ........ 14
8. Reference ........ 15

# 1. Materials and general procedures

## 1.1 Instrumentation

- **Powder X-ray diffraction (PXRD)** measurements were carried out at room temperature on a Bruker D8 ADVANCE diffractometer 40 kV, 30 mA for Cu $K\alpha$ ($\lambda$ = 1.5418 Å), with a step size of 0.05° in $2\vartheta$.
- **Thermogravimetric analysis (TGA)** measurements were performed on a SETSYS Evolution apparatus, under inert atmosphere (flow = 25 $cm^3.min^{-l}$, heating rate 5 $^oC.min^{-1}$).
- **Magnetic measurements**

  A physical property measurement system (PPMS, Quantum Design, U.S.A.) equipped with a vibrating sample magnetometer (VSM) option was employed for recording the magnetization data of the samples. In particular, the temperature dependence of sample's magnetization was measured upon warming in the temperature interval from 5 to 300 K under an external magnetic field of 1 kOe after cooling in the field of 1 kOe. The hysteresis loop of the sample was recorded in the external magnetic fields ranging from – 50 to 50 kOe at a temperature of 5 K. Prior to analysis, magnetization values were corrected considering the response of the sample holder, sample capsule, and respective Pascal constants. The dynamics of the magnetization were studied employing the superconducting quantum interference device (SQUID)-type magnetometer (MPMS-XL7 system, Quantum Design). Alternating-current (ac) magnetic susceptibility of the samples was collected in the temperature interval from 2 to 20 K in both zero and non-zero (1 kOe) static fields, oscillating fields of 1 and 3 Oe, and frequencies of the oscillating field in the interval from 10 to 1488 Hz. The experimental ac susceptibility data, normalized to the respective molar weights of the samples, were corrected for the diamagnetism estimated from Pascal's tables and sample holder calibration.

- **Scanning Electron Microscopic measurements**

  The size of and shape of crystals were studied by using Scanning Electron Microscopy (SEM, JEOL JSM-5500LV microscope). For the measurements the crystals were coated with a thin layer of platinum (~10 nm) in a BAL-TEC SCD-050 instrument.

- **Transmission Electron Microscopic measurements**

  Samples for transmission electron microscopy observation were dispersed in acetone. A droplet of the suspension was transferred onto a carbon-coated copper grid. Observation was performed on a JEOL JEM2100 microscope, and operated at 200 kV (Cs 1.0 mm, point resolution 0.23 nm). Images were recorded with a Gatan Orius 833 CCD camera (resolution 2048 x 2048 pixels, pixel size 7.4 µm) under low dose conditions.

- **Continuous rotation electron diffraction (cRED) data collection.**
  The data were collected using the software *Instamatic*.[1] A single-tilt tomography cryo-sample holder was used for the data collection, which could tilt from -70° to +70° in the TEM. *c*RED data were recorded with a Timepix pixel detector QTPX-262k (512 x 512 pixels, pixel size 55 µm, Amsterdam Sci. Ins.). The aperture used for *c*RED data collection corresponded to a selected area of about 1.0 µm in diameter. The speed of goniometer tilt was 0.90° $s^{-1}$, and the exposure time was 0.5 s per frame. Data was collected within 2 min to minimize the beam damage and to maximize the data quality. The covered tilt angle is 107.7°.

- **DFT calculation.**

  The DFT calculations were performed in the generalized gradient approximation with the Perdew–Burke–Ernzerhof functional implemented in CASTEP module of Accelrys Materials Studio. A kinetic energy cutoff of 400 eV and a Γ-centered k-point mesh of 2 × 2 × 8 were used for the calculations. The optimization of the geometry was applied by using a pseudopotential plane-wave method within the DFT framework by Accelrys Materials Studio package. After creation of the initial structure, the geometry was quick optimized in the FORCITE module with Dreiding forcefield of Materials Studio.

## 1.2 Experimental Methods

- **Synthesis of $[Cu(HCN_4)_2,(H_2O)_{2/9}],1.4(H_2O)$**
  A solution containing $Cu(NO_3)_3{\cdot}3H_2O$ (24.1 mg, 0.1 mmol), Tetrazole-5-ethylester (32.8 mg, 0.2 mmol), 4 ml $H_2O$ was prepared in a Teflon lined autoclave and heated to 125 °C for 24 h. blue crystals were harvested and air dried (Yield: 75 %).
- **Synthesis of $[Co(HCN_4)_2,(H_2O)_{2/9}],1.4(H_2O)$**
  A solution containing $Co(NO_3)_3{\cdot}6H_2O$ (29.1 mg, 0.1 mmol), Tetrazole-5-ethylester (32.8 mg, 0.2 mmol), 4 ml $H_2O$ was prepared in a Teflon lined autoclave and heated to 125 °C for 24 h. Yellow product was harvested and air dried (Yield: 70 %).

## 2. First principle calculations

With respect to Zn-MOF reported structure and experimental X-Ray data available on Cu-MOF we build different structural models (reported in Figure S2.1) changing the reciprocal position of C/N atoms on the ligands, their spatial orientation and the presence of different cations to counter balance the charges.

All the models have been geometrically optimized and we identified the most stable moiety that is reported in Figure S2.2. Figure S3.1 shows a good match between the simulated X-Ray pattern and the experimental one.

The geometry optimization and energy calculation has been done using the DFT method[2,3] with the *Vienna ab-initio simulation package* (VASP)[4,5] within the generalized gradient approximation using the Perdew–Burke–Ernzerhof (PBE) exchange–correlation functional. Core states were treated with the projector-augmented wave (PAW) method [6]. We used a 800 eV cutoff energy and dispersion forces were included with the DFT-D3 method of Grimme et al. [7]. The criteria for wavefunction and atomic forces convergence were set to $10^{-6}$ eV and 0.01 eV $Å^{-1}$, respectively. The Brillouin zone was sampled using a 2 × 2 × 2 gamma-centred mesh.

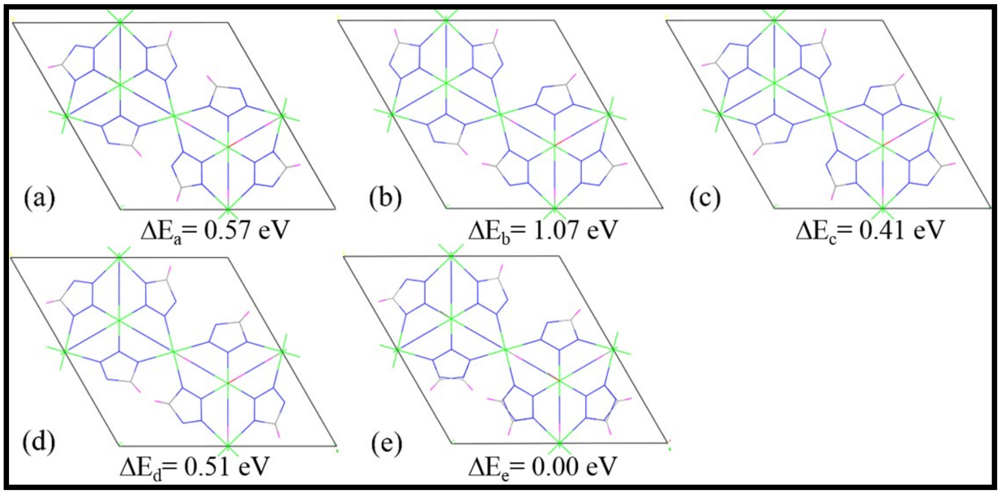

***Figure S 2.1.*** *Different configurations of C-H relative position models. (a), (b), (c) and (d) have the same configuration in the total structure, and the fifth model (e) which is the mixture of (c) and (d) by stacking these two configurations layer alternately.*

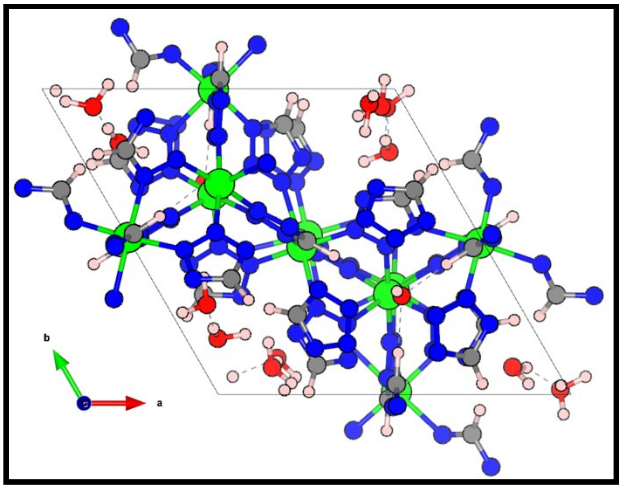

***Figure S 2.2.*** *The most stable structure from the GGA calculations.*

# 3. Structural determination and stability

SEM images show Cu-kag MOF crystals exhibited hexagonal prisms with a size of 0.7 µm x 0.7 µm x 1 µm, and Co-kag exhibited the ellipsoid crystals with a size reaching 2 µm. Because of small crystal size analysis using single crystal X-ray diffraction was not possible, hence TEM analysis by using continuous rotation electron diffraction (cRED) was applied for structural determination. Figure 1 (c & d) presents the reconstructed 3D reciprocal lattice from the cRED data that Cu-kag MOF has a primitive unit cell. The reflection conditions can be deduced as *hhl*: *l*=2*n*, 00*l*: *l*=2*n*. Thus, there are several possible space groups for Cu-kag MOF: $P6_3mc$ (No. 186), $P\text{-}6_2c$ (No. 190), and $P6_3/mmc$ (No. 194). The space group $P6_3/mmc$ with the highest symmetry was chosen for the further structural refinement. The unit cell parameters were further refined against powder X-ray diffraction (PXRD) data (λ = 1.5418 Å) using Pawley method (Figure S 3.1). The final unit cell parameters of Cu-kag MOF are a = b = 12.448 Å, c = 12.286 Å, and Co-kag MOFs are a = b = 12.392 Å, c = 12.582 Å. The simulated PXRD patterns matched well with the experimental patterns (Figure S 3.2). In detail, the peaks in $8.0^{o}$, $10.6^{o}$, and $17.7^{o}$ can be indexed as 010, 011, and 021 reflections, respectively. The peak in $13.8^{o}$ is an overlap of 002 and 110 reflections, and the peak in $16.2^{o}$ is an overlap of 012 and 020 reflections.

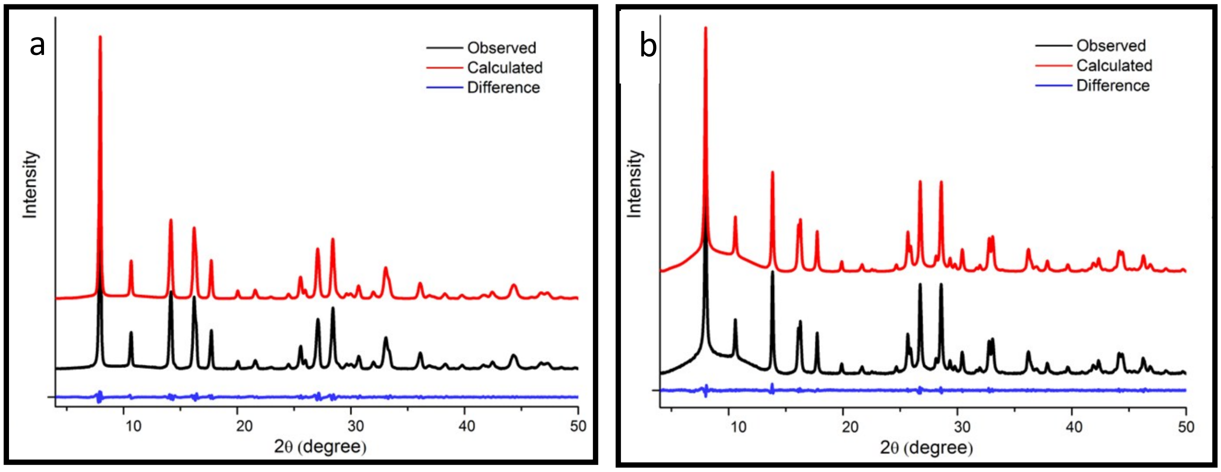

***Figure S 3.1.*** *Pawley fit of powder X-ray diffraction (λ = 1.5418 Å) for* (a) *Cu &* (b) *Co-kag MOFs. Observed data (black), calculated fit (red), and difference plot (blue).*

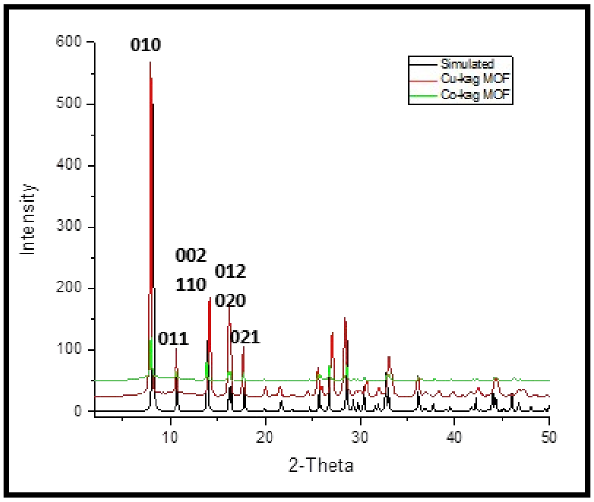

***Figure S 3.2.*** *Experimental and calculated powder X-ray diffraction (PXRD) patterns for Cu-kag (red) & Co kag-(green) MOFs in comparison with simulated pattern generated from the cif file of Zn-kag-1 reported by Eddaoudi et al.*[8]

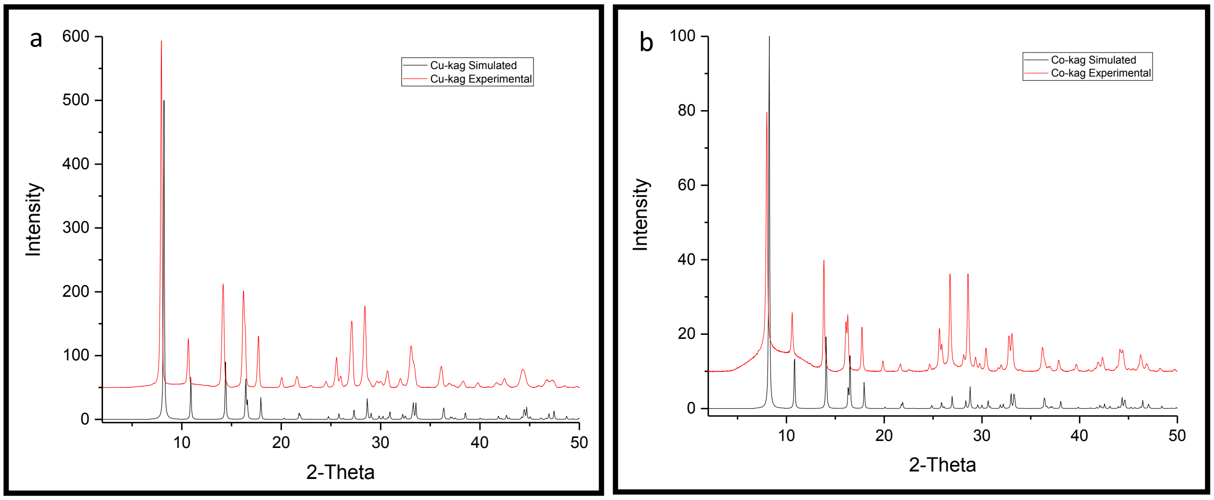

***Figure S 3.3.*** *Experimental and calculated powder X-ray diffraction (PXRD) patterns for (a) Cu-kag & (b) Co kag-MOFs, indicating the phase purity of the as-synthesized sample.*

This compound has a very good stability towards water (even after 24 hours in boiling water) as well as in many other organic solvents. The stability of the as-synthesized MOF was proved at different pH levels (pH 1 and pH 12 in *Cu-kag* MOF & pH 1 and pH 14 in Co-*kag* MOF).

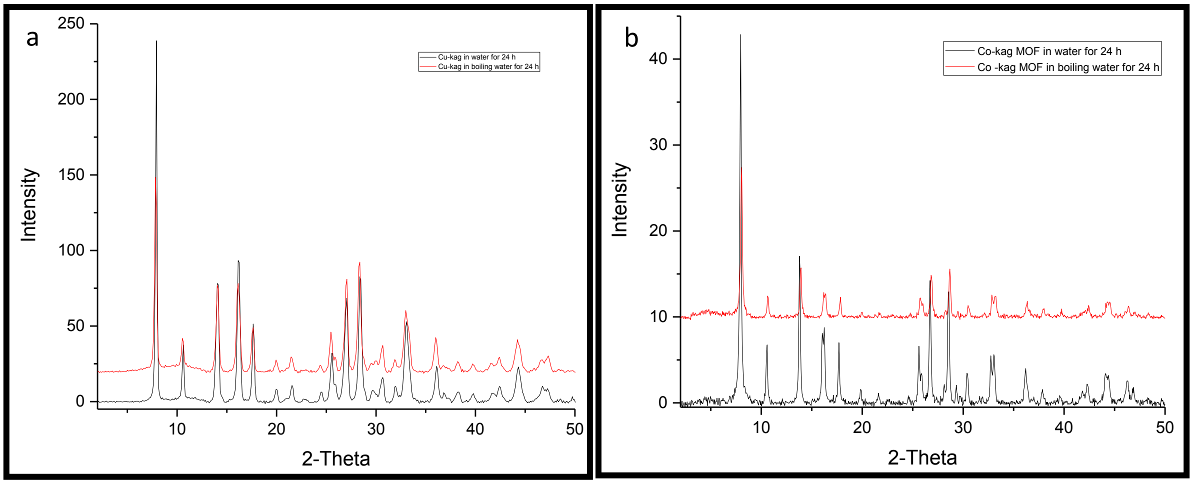

***Figure S 3.4.** Stability in water and boiling water after soaking for 24h(a) Cu-kag (b) Co-kag* MOFs.

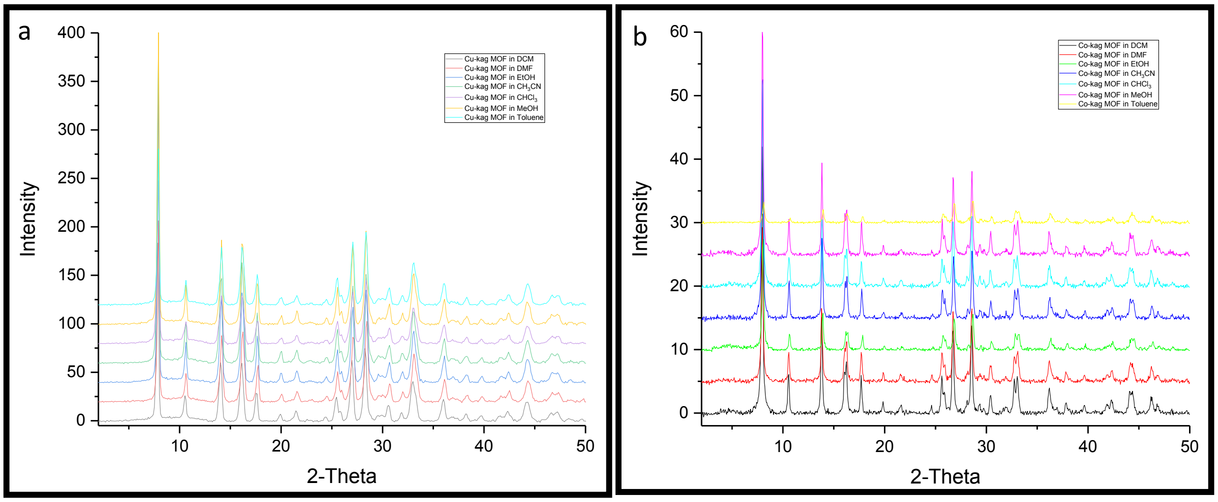

***Figure S 3.5.** Stability in different solvents for 24 h (a) Cu-kag and (b) Co kag* MOFs.

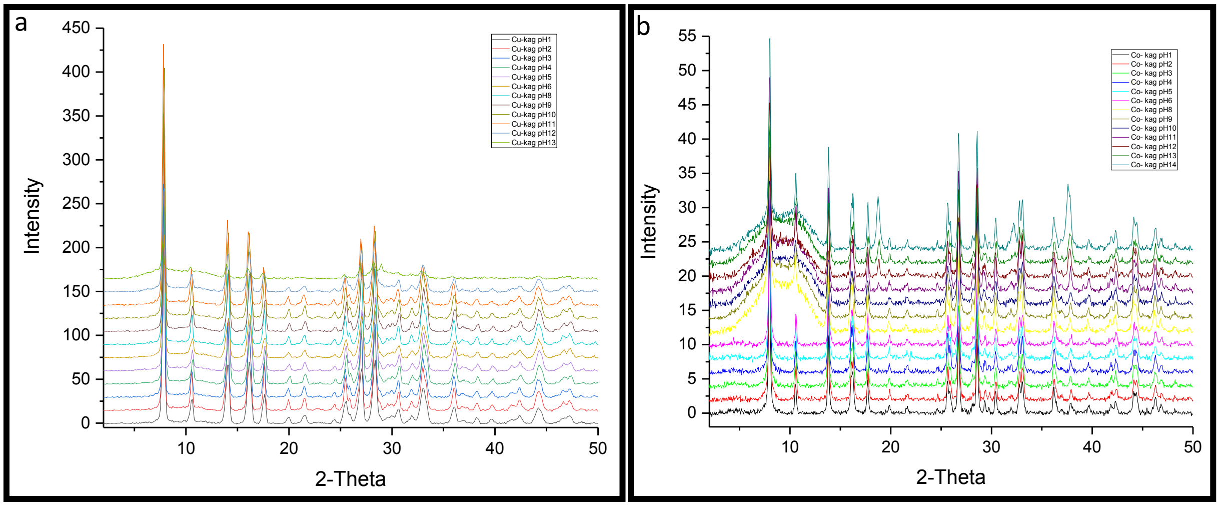

***Figure S 3.6.*** *Stability at different pH of (a) Cu-kag and (b) Co-kag* MOFs.

**Table S1.** Crystallographic data and Powley fit results of Co- and Cu-kag MOFs.

| | Co-kag MOF | Cu-kag MOF |
|---|---|---|
| Chemical formula | $C_6H_6Co_3N_{24}$ | $C_6H_6Cu_3N_{24}$ |
| Formula weight | 591.14 | 605.00 |
| Crystal system | Hexagonal | Hexagonal |
| Space group | $P6_3/mmc$ | $P6_3/mmc$ |
| *a*/Å | 12.3917(2) | 12.4479(5) |
| *c*/Å | 12.5816(2) | 12.2856(4) |
| Temperature/K | 298(2) | 298(2) |
| Wavelength/Å | 1.5418 | 1.5418 |
| $2\vartheta$ range/° | 3.99– 50.00 | 3.99– 50.00 |
| R*p* | 0.0386 | 0.0633 |
| R*wp* | 0.0399 | 0.0634 |
| R*exp* | 0. 0287 | 0. 0771 |
| GOF | 1.388 | 1.082 |

## 4. Thermogravimetric analysis

The PXRD analysis of the residue reveals the formation of CuO/CoO from of the framework degradation. The initial weight loss is attributed to the departure of water molecules.

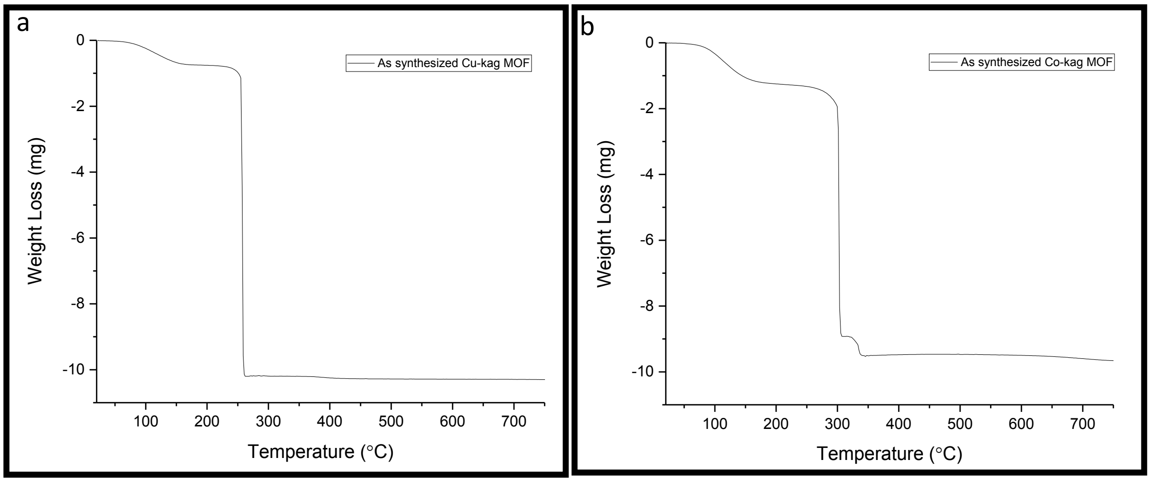

***Figure S 4.1.*** *Thermogravimetric analysis of (a) Cu-kag and (b) Co-kag* MOFs.

## 5. AC Magnetic Susceptibility Measurements

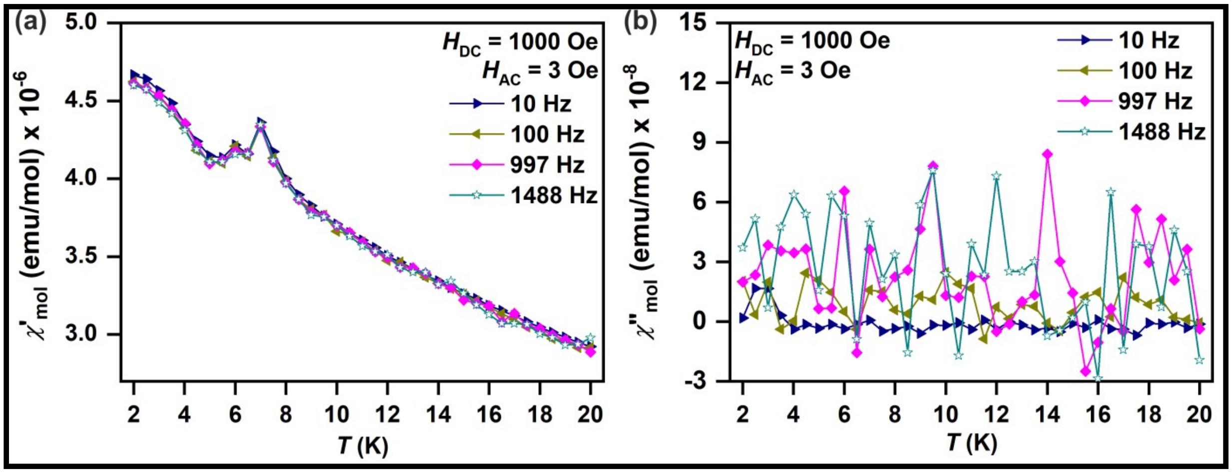

***Figure S 5.1.*** *The temperature dependence of (a) in-phase (χ'$_{mol}$) and (b) out-of-phase (χ''$_{mol}$) alternating-current (ac) molar susceptibility of the Co-kag sample, recorded at a static field of 1 kOe, oscillating field of 3 Oe, and frequencies of the alternating field from 10 to 1488 Hz.*

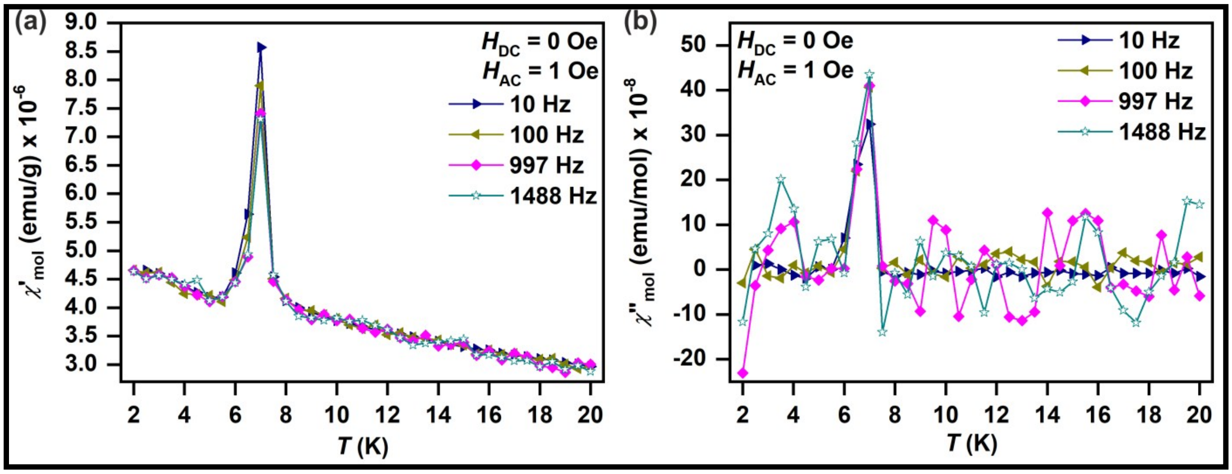

***Figure S 5.2.*** *The temperature dependence of (a) in-phase (χ'$_{mol}$) and (b) out-of-phase (χ''$_{mol}$) alternating-current (ac) molar susceptibility of the Co-kag* MOF *sample, recorded at a zero static field, oscillating field of 1 Oe, and frequencies of the alternating field from 10 to 1488 Hz.*

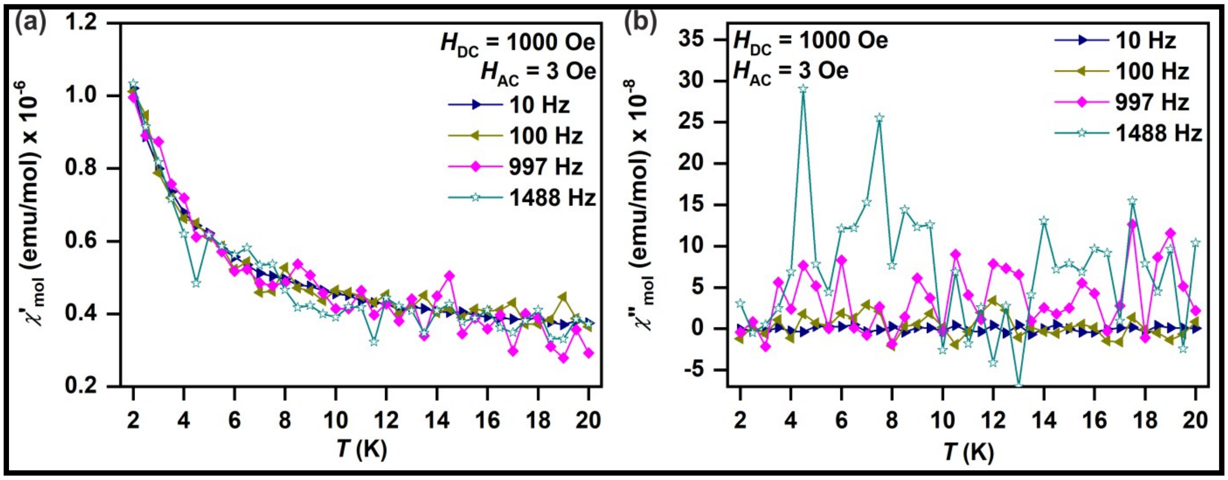

***Figure S 5.3.*** *The temperature dependence of (a) in-phase ($\chi'_{mol}$) and (b) out-of-phase ($\chi''_{mol}$) alternating-current (ac) molar susceptibility of the Cu-kag* MOF *sample, recorded at a static field of 1 kOe, oscillating field of 3 Oe, and frequencies of the alternating field from 10 to 1488 Hz.*

## 6. Electronic Structure

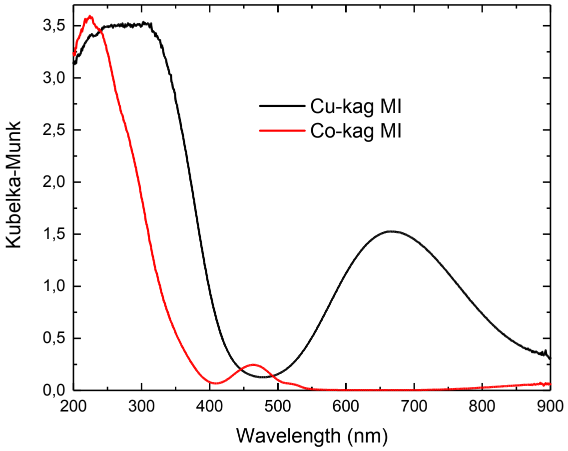

***Figure S 6.1.*** *UV-Vis spectra of Cu & Co kag MOF*

Due to the band-gap problem the PBE functional is not suitable to describe the electronic properties. We combine hybrid functional with the Hubbard *U* scheme to calculate the electronic structure.[9] The results are reported in Figure S 6.2. From the analysis of Figure S 6.2, PDOS we can observe how the frontiers states, which are responsible for magnetic properties, are formed by the overlap of the metallic orbitals with the ligand one. With the same methodology we also try to determinate a reference magnetic state, but we did not manage to converge a specific magnetic configuration.

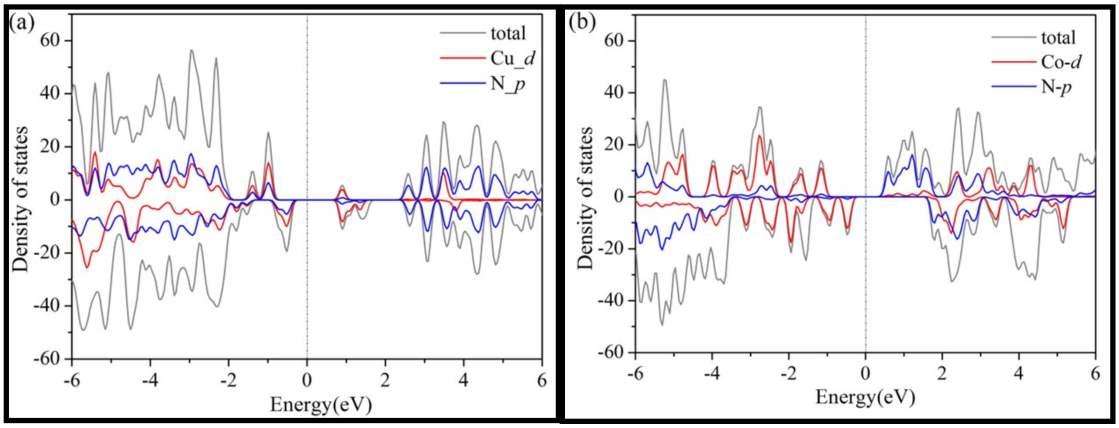

***Figure. S 6.2.*** *Project density of states (PDOS) of HSE+U for Cu & Co- kag MOFs. Cu- kag MOF PDOS (a) and Co- kag MOF PDOS (b).*

## 7. Low-Pressure Gas Adsorption Measurements

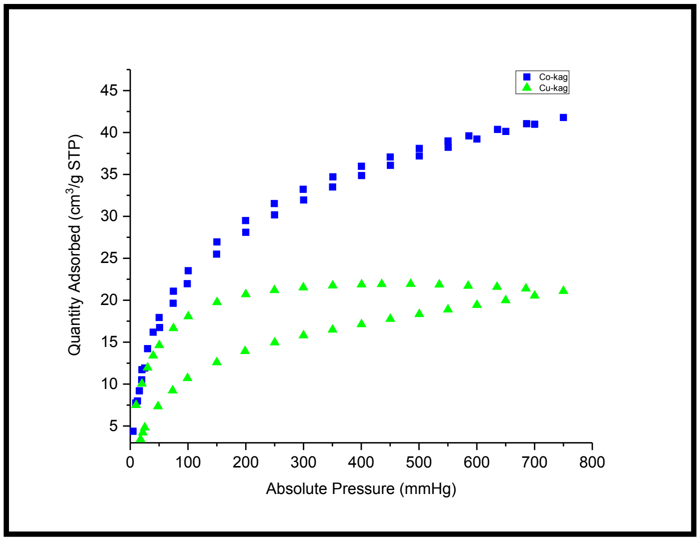

***Figure. S 7.1.*** *$CO_2$ adsorption isotherms on Co & Cu-kag MOFs at 293 K after evacuation at 423 K.*

## 8. Reference

1. M. O. Cichocka, J. Ångström, B. Wang, X. Zou, S. Smeets, *J. Appl. Crystallogr.* **2018**, *51* (6), 1652–1661.
2. P. Hohenberg, W. Kohn, *Physical Review* **1964,** *136* (3B), B864-B871.
3. W. Kohn, L. J. Sham, *Physical Review* **1965,** *140* (4A), A1133-A1138.
4. G. Kresse, J. Furthmüller, *Physical Review B* **1996,** *54* (16), 11169-11186.
5. G. Kresse, J. Furthmüller, *Computational Materials Science* **1996,** *6* (1), 15-50.
6. P. E. Blöchl, *Physical Review B* **1994,** *50* (24), 17953-17979.
7. S. Grimme, J. Antony, S. Ehrlich, H. Krieg, *J. Chem Phys* **2010,** *132* (15), 154104.
8. M. I. H. Mohideen, R. S. Pillai, K. Adil, P. M. Bhatt, Y. Belmabkhout, A. Shkurenko, G. Maurin and M. Eddaoudi, *Chem-Us*, 2017, **3**, 822-833.
9. M. Aras, C. Kilic, *J Chem Phys* **2014,** *141* (4), 044106.